



Observations of geostrophic transport variability in the western tropical Indian Ocean

J. R. DONGUY* and GARY MEYERS†

(Received 15 September 1993; in revised form 29 September 1994; accepted 10 November 1994)

Abstract—Dynamic height was calculated from XBTs collected along several shipping routes in the western Indian Ocean. In the northern hemisphere, low dynamic heights prevail during the NE monsoon and high dynamic heights during the SW monsoon inducing an alternating Somali Current. In the southern hemisphere, at 7°–8° S a trough of low dynamic height occurs during the whole year. EOF analysis is used to document the variation of these features. The geostrophic transports calculated for the XBT routes show spatially coherent patterns with strong seasonal variations. In the Arabian Sea, an anticlockwise gyre develops during the NE monsoon alternating with a clockwise gyre during the SW monsoon. Between 5°N and 5°S, the transport variations show eastward flow twice each year during the monsoon transitions, except on the westernmost route where the annual variations of the gyre in the Arabian Sea extend to the equator. The mean transport of the South Equatorial Current increases regularly with longitude from east to west in all months. It has small annual variations, and the phase of the annual maximum progresses consistently westward.

1. INTRODUCTION

It is recognised that the southern hemisphere oceans are less sampled and less studied than the northern hemisphere oceans. This is particularly true for the southern Indian Ocean. Observations collected recently under auspices of the international Tropical Oceans and Global Atmosphere (TOGA) programme and the World Ocean Circulation Experiment (WOCE) have added substantially to the large scale coverage of thermal (baroclinic) structure.

Historical observations tended to be sparse, or highly localized. The International Indian Ocean Expedition was carried out during 1962–1965 (Wyrski, 1971) and showed that the northwestern Indian Ocean, is dominated by the monsoon. The strong response in ocean currents attracted a number of studies through the 1970s and early 1980s that focused on the currents and eddies off the coast of Somalia. The results have been comprehensively reviewed by Knox (1987). A highlight was the description by Duing *et al.* (1980) and Swallow and Fieux (1982), who pointed out the behaviour of the surface flow of the Somali Current, which sometimes forms two gyres off the eastern coast of Africa. The study of western boundary currents was extended to southern latitudes by Donguy and Piton (1991), showing that circulation in the Mozambique Channel is also characterised by a seasonal cycle of meridional transport in phase with the monsoon cycle. The East African

*Centre ORSTOM de Brest, B.P. 70, 29280 Plouzane, France.

†CSIRO Division of Oceanography, GPO Box 1538, Hobart, TAS 7001, Australia.



Current and other boundary currents located in the vicinity of Madagascar have been described by Swallow *et al.* (1988), Schott *et al.* (1988) and Swallow *et al.* (1991), who document the transport, the seasonal regime and the possible monsoon influence.

The large scale description of currents, including the early works of Wyrtki (1973a,b) and the recent studies by Reverdin (1987) and Molinari *et al.* (1990), used surface-drift measurements to generate a monthly climatology of surface currents. They documented reversing monsoon currents, particularly in the northern hemisphere, and strongly semiannual variations in the current on the equator. These studies were representative primarily of the directly wind driven currents. Variation in subsurface thermal structure associated with the monsoons was described by Colborn (1975). Hastenrath and Greischar (1991) used historical oceanographic observations from atlases to define the pattern of currents and the influence of the monsoon on large scale surface currents, including a partition into geostrophic and wind driven components. Woodberry *et al.* (1989), using a reduced gravity-model, found that the main feature in the southern hemisphere is a cyclonic gyre including the South Equatorial Current and South Equatorial Counter-current.

This study is concerned with a large scale description of upper layer transports in the Arabian Sea and western tropical Indian Ocean using new expendable bathythermograph (XBT) data. It extends the earlier climatological studies by focusing on the upper ocean, geostrophic circulation which develops in response to monsoon winds. The observations were made routinely and systematically during a period of three years, 1986–1989. Guidelines for XBT sampling in the TOGA and WOCE Programmes were based on optimal interpolation (Phillips *et al.*, 1990; Meyers *et al.*, 1991; Meyers and Phillips, 1992).

2. DATA AND DATA PROCESSING

Since 1983, the TOGA/WOCE XBT Programme in the Indian Ocean has been gradually extended by Australia (CSIRO), France (ORSTOM) and Japan (JMA) over the following routes: Port Hedland (20°S, 118°E)–Japan (since 1985), Fremantle–Sunda Strait (since 1983), Fremantle–Persian Strait (since 1986), Fremantle–Red Sea (since 1986), Red Sea–Reunion Island (21°S, 55°E) (since 1985).

The first two routes cover the eastern Indian Ocean and have been used for studies of the Pacific–Indian Ocean throughflow (Meyers, 1992; Meyers *et al.*, 1995). The three last routes cover the western Indian Ocean, (20°S–25°N, 50°E–90°E) and are used for the present study. Sampling on the northern end of the route to the Persian Gulf was stopped near 17°N in the early years of the programme due to the Iran–Iraq War. The TOGA/WOCE XBT Programme added several additional lines to the Indian Ocean after 1989 which are not included in this study. Sampling on a line along the eastern coast of Africa was unfortunately stopped before the TOGA programme began, and was subsequently started again. Clearly, a climatology based on much more data can be prepared at the end of TOGA; however, the data collected during the first years is enough to produce a representative climatology which will be useful for descriptive purposes and for the validation of general circulation models which are being developed.

XBTs provided temperature profiles from the surface to 450 m (or more) every 60–90 miles along the routes, but sometimes more. Bimonthly, averaged values of temperature at standard depths, dynamic height and the geostrophic transport function relative to 400 dB have been computed to study qualitatively and quantitatively the distribution of

currents during a standard year. The data used for the climatology covered mainly the period 1985 through 1989. Preparation of the climatology is described in detail in a report (Meyers *et al.*, 1994b). Briefly, the averages along a route were calculated in bins of one degree of latitude, except near coastal boundaries where bins were adjusted to have one in shallow water (<500 m) when possible. With the exception of one line, no spatial smoothing was permitted so that the consistency of the seasonal cycle in adjacent bins could be checked. The Fremantle–Persian gulf line was processed with overlapping 3° latitude bins because it was not covered as consistently as the others. The averages were calculated for bimonths with a one month overlap (January–February, February–March, etc.). Dynamic height and the transport function were calculated from the bimonthly averaged temperature using the climatological temperature/salinity relationship (Levitus, 1982). The dynamic height-profiles along the routes were presented in a preliminary study by Donguy and Meyers (1992).

The XBT lines cross several major currents including the Somali Current, the Indian Monsoon Current (North Equatorial Current), the semiannual Equatorial (Wyrcki) Jets, the South Equatorial Current and the South Equatorial Countercurrent. The bimonthly averaged transport of the currents was estimated from differences in the transport function. Most of the paper is concerned with a description of the annual and semiannual variations in transports.

3. ERROR DISCUSSION

The error in estimating longterm, bimonthly averaged transports is largely due to the statistical errors associated with small scale variability which is not well resolved by the XBT sampling, such as eddies and internal waves, or due to seasonal variation of the T/S relationship. Both of these errors are discussed below.

The statistical error was estimated from propagation of error formulae (Ku, 1966) and statistics on the variability of subsurface temperature on the TOGA/WOCE XBT lines (Phillips *et al.*, 1990). This approach is necessary because the transports were calculated from bimonthly averaged temperature sections. A two layer model of the ocean tuned to exactly represent the longterm annual mean transport of each current was used to facilitate the propagation of error.

In a two layer model with the bottom layer at rest the transport (T) of a current is:

$$T = \frac{g'}{2f} (D_N^2 - D_S^2) = C(D_N^2 - D_S^2) \quad (1)$$

where D_N and D_S are the depth of the interface on the northern and southern edges of the current, g' is the reduced acceleration of gravity and f is the Coriolis parameter. The value of C was chosen so that the correct annual mean transport of each current is produced by the annual mean depths of the 20°C isotherm given by Phillips *et al.* (1990) for the interface depth. (C was estimated for the maximum northward current in the case of the Somali Current.). The problem is to determine the standard error (E_T) of bimonthly mean transports, given information on the mean and standard deviation of interface depths. From Ku (1966),

$$E_T = \frac{2C\sigma}{\sqrt{n}} ((D_N)^2 + (D_S)^2 + 2\sigma^2)^{1/2} \quad (2)$$

Table 1. Standard error (E_T) 10^6 m³/s (Sv) of the bimonthly mean transports estimated for the South Equatorial Current (SEC), the South Equatorial Counter Current (SECC) and the Somali Current (SC); and estimates of the constant C from equation (1)

Track	Current		SEC		SECC		SC	
	No. XBTs	No. transects	C m/S	E_T Sv	C m/S	E_T Sv	C m/S	E_T Sv
Fremantle Persian Gulf	1920	40	873	2.6	2211	5.5	No data	
Fremantle Red Sea	1898	42	700	2.2	1945	4.2	813	2.5
Red Sea La Reunion	2343	69	683	1.7	2205	3.5	905	2.1

where (D_N) and (D_S) are the annual mean depths, σ is the standard deviation of D_N and D_S (assumed to be equal) and n is the number of transects across the current during a bimonth. The derivation of this formula assumes that variations of D_N and D_S are not correlated.

The results of calculations with (1) and (2) are in Table 1, which also shows the total number of XBT drops on each line and the number of transects obtained during the study period. The standard error of bimonthly mean transport is in the range 2 to 5×10^6 m³/s, depending mainly on the current. The values of C are strongly influenced by the choice of 20°C to represent the depth of the interface. The standard errors are generally smaller than the variations in transport described later, except possibly for the South Equatorial Countercurrent. By the end of TOGA the number of transects on the lines will increase by a factor of two to three, further reducing the statistical error in the longterm bimonthly mean transports.

Statistical errors due to small scale variations in the T/S relationship generally have a small effect on the calculation of dynamic height and geostrophic transports. For example, RMS errors in dynamic height due to using a mean T/S relationship are often in the range of two to four dynamic cm (Hastenrath and Greischar, 1991; Taft and Kessler, 1991, Appendix A3), which is much smaller than the variations due to eddies as discussed above.

A more important aspect of the T/S relationship is the possibility that there are systematic, seasonal variations, that if neglected create a bias in our results based on the annual mean T/S relationship. A complete study of the T/S relationship in the whole domain of the XBT network is beyond the scope of this paper, and could be seriously flawed by the limited number of salinity observations in the Indian Ocean. In order to estimate the possible magnitude of the effect of seasonal salinity variations, we have carefully looked at the seasonal salinity data of Levitus (1982) on one XBT line (Fremantle-Red Sea). Seasonal variations of salinity were found at the surface, but these have only a small effect on dynamic height because they develop in a shallow layer of typically 50 m or so. The subsurface variations of T/S relationship were small over most of the track, consistent with aliasing of the small scale variability discussed above. Apparently systematic seasonal variations were, however, found in the latitude band 18°S to 12°S. These variations could be associated with meridional shifts in the salinity front usually found in this latitude band. We found that the seasonal change in salinity could

affect the calculation of transport in the South Equatorial Current by as much as 5×10^6 m^3/s . A potential bias of this magnitude should be kept in mind for any application of the results on transports presented later.

4. SEASONAL VARIATIONS OF DYNAMIC HEIGHT

According to the general description of the surface circulation in the western tropical Indian Ocean by Wyrski (1973a) and Molinari *et al.* (1990), the region is characterized by reversals of the major currents in response to monsoons. The currents with the strongest monsoonal variation are the Somali Current (SC), which flows strongly northward along the coast of Africa during the SW monsoon (June to September) and southward during the NE monsoon (December to February); and the North Equatorial Current (NEC) south of India, which flows westward during the NE monsoon and eastward during the SW monsoon, when it is sometimes called the Indian Monsoon Current (IMC). Annual variation without reversal was also noted in the South Equatorial Countercurrent (SECC) and the South Equatorial Current (SEC). The SEC and SECC form a distinct gyre in the southern hemisphere (Molinari *et al.*, 1990). Bimonthly charts of the surface dynamic height relative to 400 dB determined from the XBT data (Figs 1 and 2) indicate a circulation pattern which is generally consistent with this scheme; however closure of the gyres at the western boundary cannot be seen because of the lack of data near the coast of Africa.

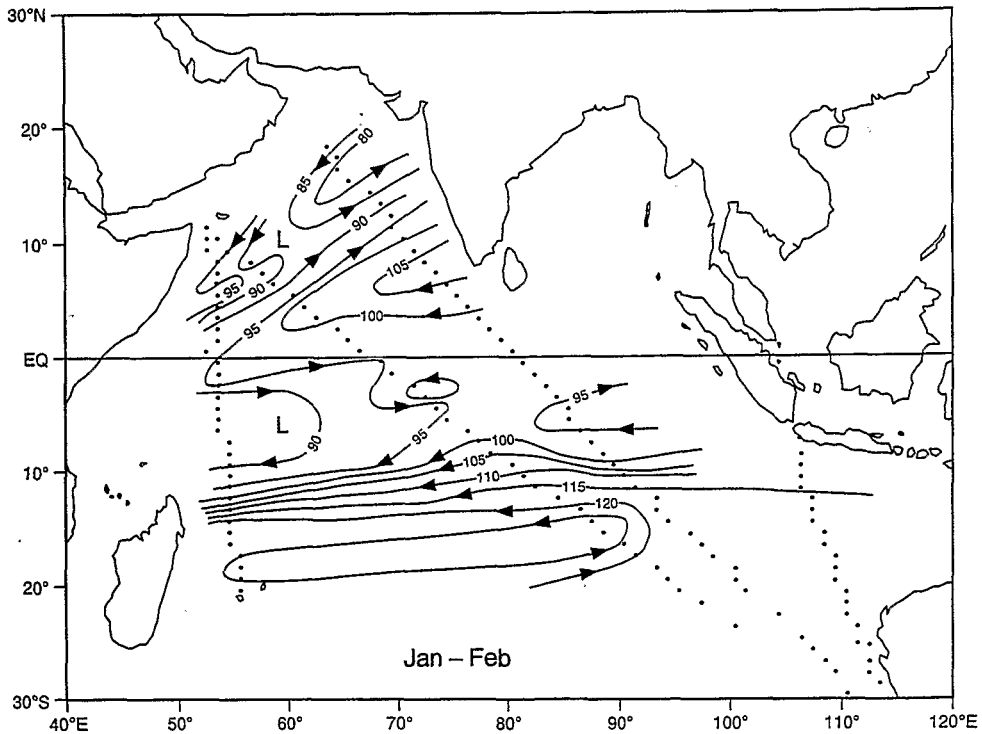


Fig. 1. Surface dynamic height relative to 400 dB in dynamic millimetres for January/February.

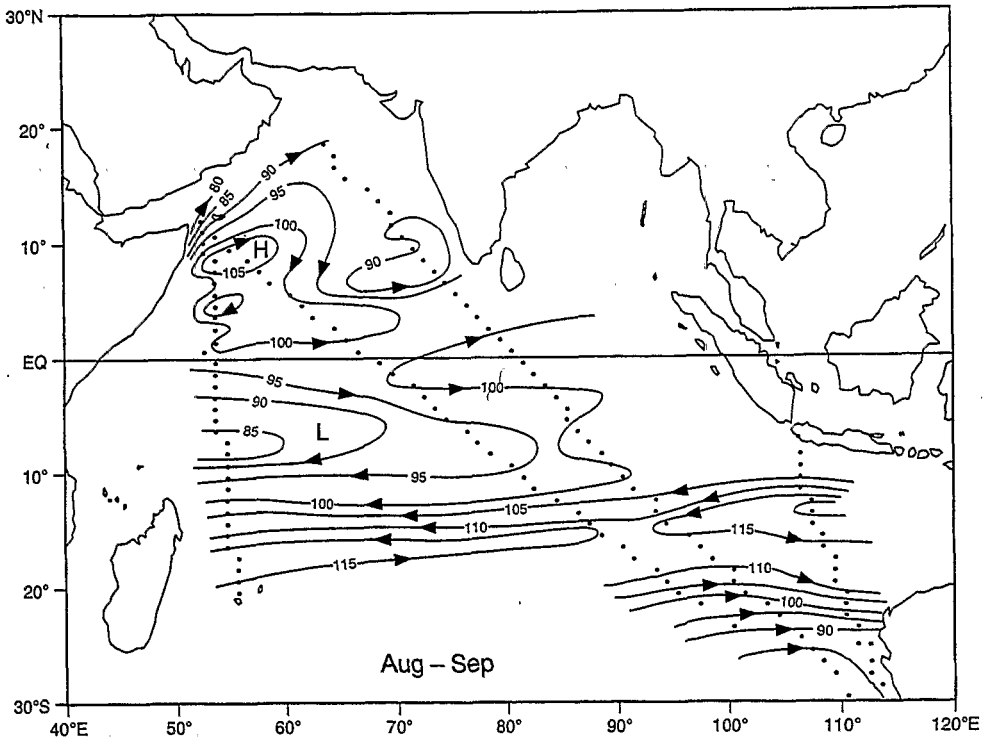


Fig. 2. Surface dynamic height relative to 400 dB in dynamic millimetres for August/September.

The charts show that dynamic height in the Arabian Sea from December to February is characterised by a low indicating counterclockwise circulation and by the southwestward SC along the African coast (Fig. 1). The low is associated with the presence of cool, saline water originating from the Arabian Sea in the northern winter during the NE monsoon (Donguy, 1974). The full sequence of charts (not presented) shows that the low is a transient phenomenon and is quickly replaced by a high in March. A broad low in the southern hemisphere near 8°S is the trough between the SEC and the SECC. The trough extends into the central Indian Ocean, which might be expected due to the usual location of the Intertropical Convergence Zone (ITCZ) south of the equator in this season (Sadler *et al.* 1987), but it is a weak feature. Bimonthly dynamic height charts from the International Indian Ocean Expedition (Wyrтки, 1971) present a similar pattern for the season of the NE monsoon.

The dynamic height from June to October during the SW monsoon is characterised by a strong high in the Arabian Sea and again the low SECC trough in the southern hemisphere (Fig. 2). The high indicates clockwise circulation around a gyre in the Arabian Sea and the northeastward Somali Current. The maximum dynamic height is located near 10°N and includes the Great Whirl described by Swallow and Fieux (1982). At least during the mature monsoon, the high is associated with warm, low salinity water coming from the equatorial area of the western Indian Ocean (Donguy, 1974). The high is a more persistent feature than the previous low, lasting five months instead of three. The trough between the SECC and SEC clearly extends into the central Indian Ocean in this season. The SECC

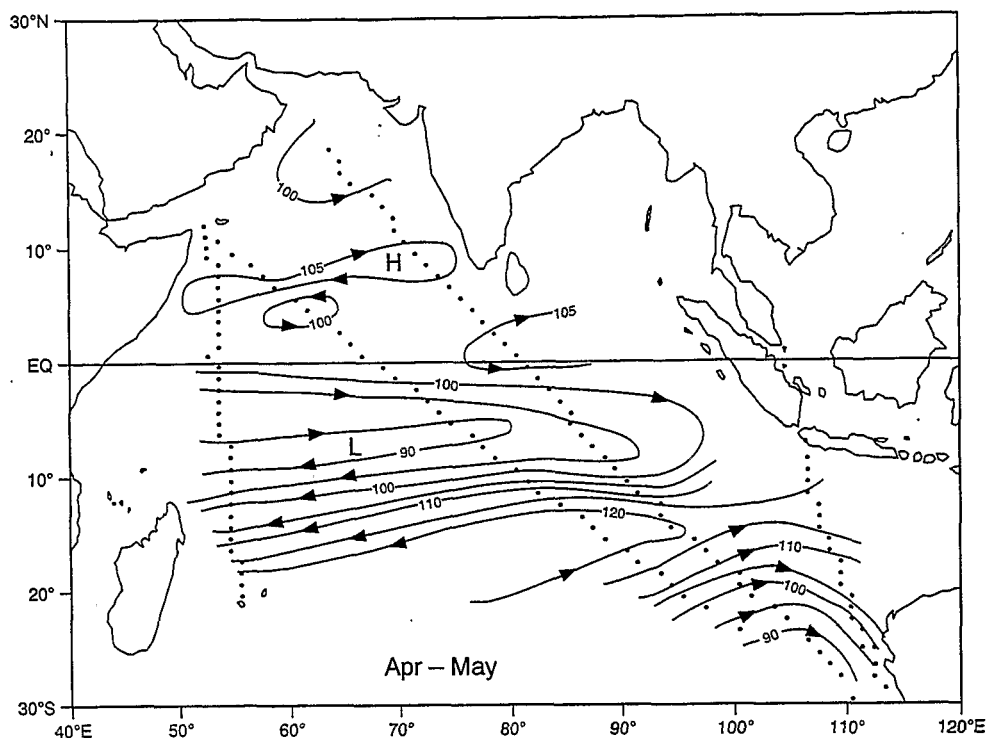


Fig. 3. Surface dynamic height relative to 400 dB in dynamic millimetres for April/May.

flows against the prevailing wind and in this sense appears to be dynamically similar to the Countercurrent in the Pacific Ocean (Meyers, 1979). Bimonthly dynamic height charts from Wyrтки (1971) present a similar pattern for the SW monsoon also.

The complete set of dynamic height maps showed that the SECC trough has maximum eastward extension during the transition season April–May (Fig. 3), reaching at least 90°E. This feature may be related to the presence of the ITCZ at 10°S for five months, and it comes at the end of the season of westerly winds between the equator and 10°S. The SECC flows in the direction of the wind during the five months. Again, the appearance of the trough in this season is in good agreement with Wyrтки (1971). The high dynamic height of the Arabian Sea has already developed by April–May and suggests a clockwise circulation including the NEC and the SC.

The variation of dynamic height throughout the year was represented by empirical orthogonal functions (EOF) using the data for all the XBT lines listed above. The EOF results west of 90°E are presented to document the annual variation in the Arabian Sea and tropical Indian Ocean. The EOF results (Figs 4 and 5) show temporal variation with peak monsoon development near January–February and July–August, and a secondary peak in the first EOF in April–May. The dynamic height fields at these times were presented Figs 1–3.

The first EOF (Fig. 4) represents primarily variations of the monsoon gyre north of the equator and a change in the meridional slope of dynamic height across the SECC and SEC. It accounts for 43% of the monthly variance. The associated time function describes one

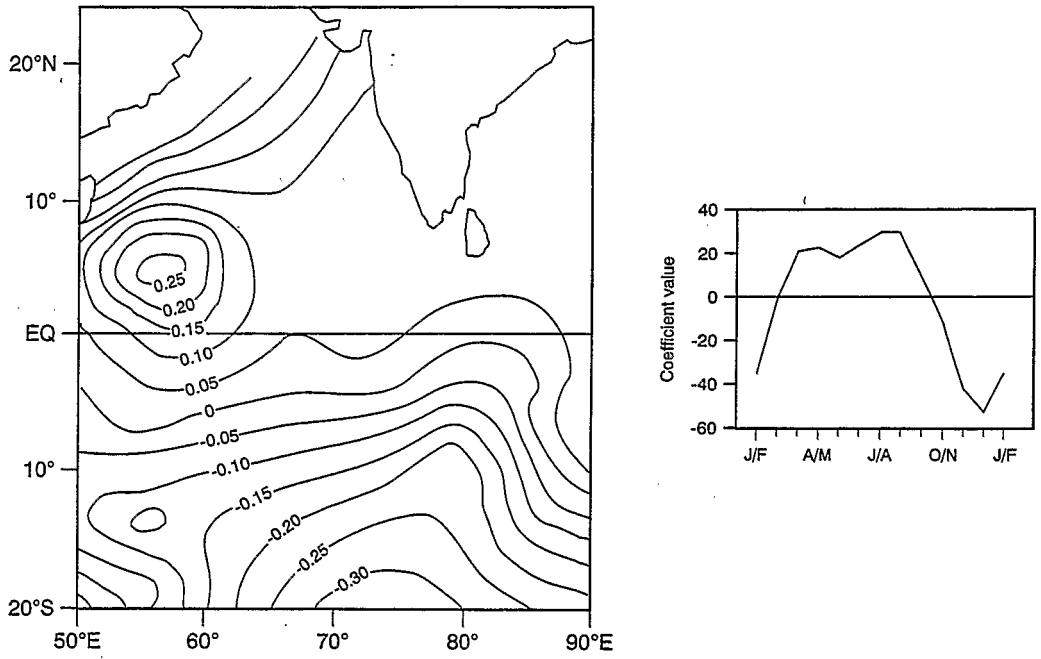


Fig. 4. Eigenvector 1 and associated time function of the dynamic height relative to 400 dB.

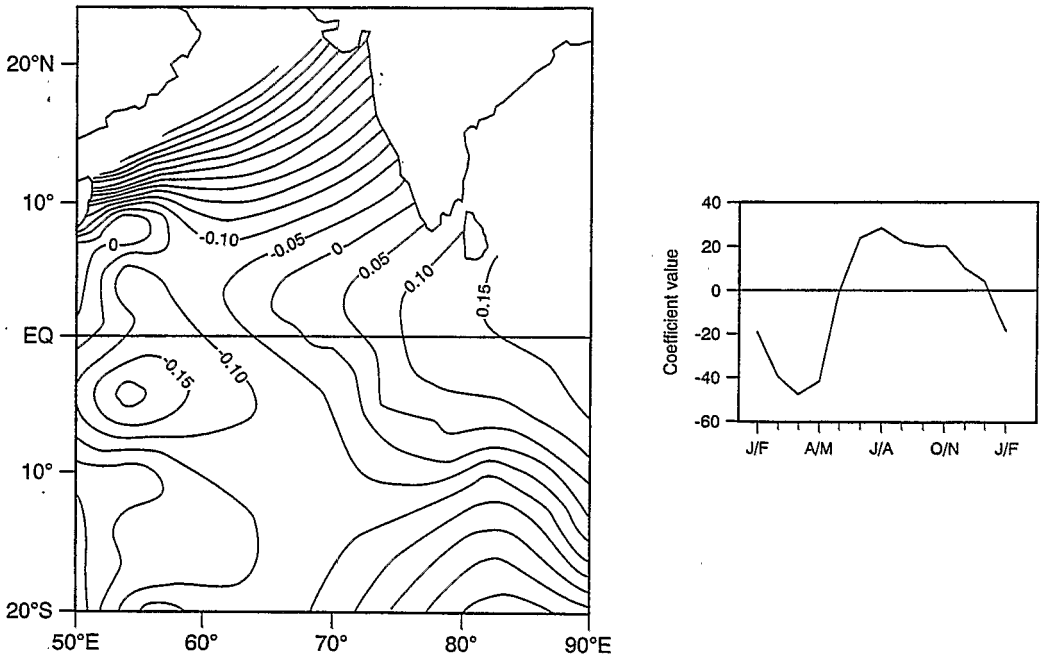


Fig. 5. Eigenvector 2 and associated time function of the dynamic height relative to 400 dB.

asymmetric cycle per year, which shows the longer persistence of the pattern of circulation for the SW monsoon, and the rapid formation and decay of the pattern for the NE monsoon. From March through October, a high deviation from the mean dynamic height develops at 5°N , 55°E , representing the centre of variation of the gyre. The circulation around this core is clockwise in this season and shows the conspicuous North–Eastward Somali Current. South of the equator, the eastward current is strengthened in both the western and central Indian Ocean. This pattern appears to begin in March/April before the onset of the SW monsoon suggesting that its dynamic is not controlled by the local wind. The EOF suggests that the anticlockwise circulation during the NE monsoon develops for a relatively short period from November through February.

The second EOF shows dynamic height variations concentrated near the western boundary particularly in the northern hemisphere. It represents 34% of the variance (Fig. 5). It seems to represent the patterns during the peak and mature phases of the monsoons. The pattern is largely devoted to the Somali Current and the SECC trough on the routes closest to the western boundary. The third EOF (not presented) represents 10% of the variance and seems also devoted to the Somali Current. The associated time function describes two cycles per year.

5. SEASONAL VARIATIONS OF THE 0–400 DB TRANSPORT

The large scale Indian Ocean circulation was described by Wyrtki (1973a) and Molinari *et al.* (1990) using primarily surface drift currents. The XBT data can be used to document the associated, relative geostrophic flow in the layer 0–400 m. The boundaries of major currents were identified in the geostrophic transport function along the tracks for each bimonth and the volume transport relative to 400 dB was then calculated, (Figs 6 and 7, dots show the boundaries of currents). The transports between 0.5°N and 0.5°S were ignored. Use of the differential form of the geostrophic relationship was rejected for this study because the three-year averages are still too noisy to calculate second derivatives of dynamic height. The transport between 0.5°S – 2.5°S was considered as the southern component of the equatorial jets and the transport between 0.5°N – 2.5°N as its northern component. The transport of the Somali Current on the lines to the Red Sea was assessed between 11.5°N and 7.5°N on the northern side of the gyre in the Arabian Sea. The transport of the return flow on the southern side of the gyre was assessed between 2.5°N and 7.5°N . The boundaries of the gyre were shifted to the north slightly on the Fremantle–Persian Gulf line. The NEC/IMC was assessed on the Persian Gulf line south of Sri Lanka between 2.5°N and 7.5°N . The SEC was assessed between the subtropical ridge in dynamic height and the SECC trough. The SECC was assessed between 2.5°S and the SECC trough. The maps show transports during the peak monsoon seasons in $10^6 \text{ m}^3/\text{s}$ (Sverdrups, Sv), and arrows indicate the direction of flow inferred from the maps of dynamic height.

The transports for January/February (Fig. 6) show all of the major currents for the NE monsoon season discussed by Molinari *et al.* (1990). The anticlockwise circulation in the Arabian Sea is the dominant feature north of the equator. The gyre is a coherent feature on all the transport maps for December to February (not presented), suggesting a relative gyre-transport during the peak monsoon of approximately 10 Sv. In February/March (not presented) the transport around the gyre weakens to 7 Sv. This gyre can also be seen in the transport maps of the Indian Ocean Atlas (Wyrtki, 1971, p. 382). The NEC

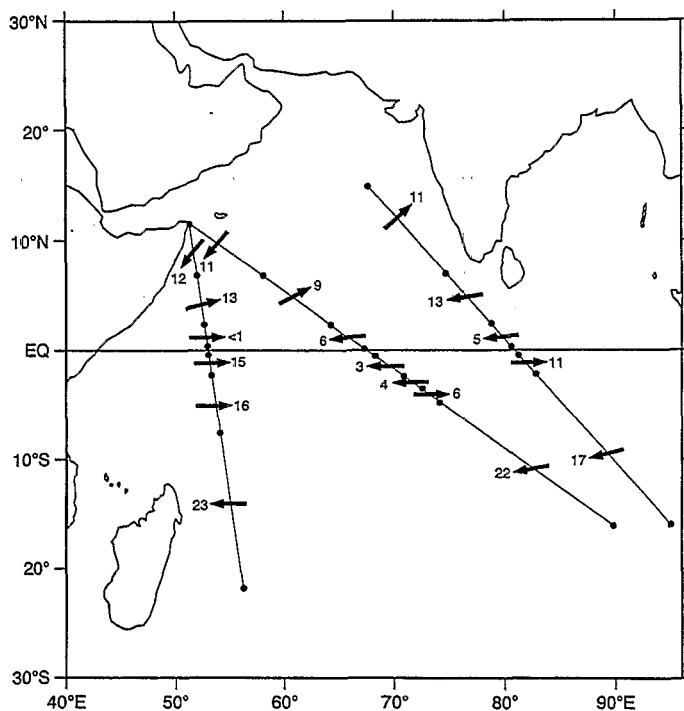


Fig. 6. Transport in Sverdrups ($10^6 \text{m}^3/\text{s}$) relative to 400 dB in January/February.

flows westward south of the gyre and seems to turn north-eastward near 60°E to join the gyre. The SEC flows westward with a relative transport increasing to 23 Sv. A large part of it may join the SECC, which has a relative transport of 16 Sv on the westernmost track. Curiously, the SECC is a weak current on the two tracks in the central Indian Ocean throughout the period January to March, suggesting that much of the flow in the SEC/SECC gyre recirculates near the western boundary (Molinari *et al.*, 1990). Erratic estimates of transport near the equator in Fig. 6 may be in part due to the aliasing of eddy variability.

The transport map for August/September also shows all of the major currents for the season (Fig. 7). From July to October, the circulation pattern shows a clockwise gyre in the Arabian Sea, intensified in the west, in the feature historically called the Great Whirl (GW). The gyre appears as a coherent feature on all the transport maps from July through October (not presented) with a typical relative transport of 20 Sv circulating around the GW. The gyre shifts measurably northward during the SW monsoon and by September is located entirely north of 5°N . Again, the gyre-transports during the peak monsoon (Fig. 7) are in agreement with the Indian Ocean Atlas (Wyrki, 1971, p. 385); and the circulation pattern is consistent with later studies of the Somali Current (Swallow and Fioux, 1982). Outflow from the eastern end of the gyre seems to feed the IMC (Fig. 2). In the southern hemisphere the SECC is strong (19 Sv) on the westernmost line and considerably weaker in the central ocean, again suggesting recirculation. Transport of the SEC is about 20 Sv, as it was during the opposite monsoon. Erratic estimates appear near the equator.

Time series (Figs 8–12) were prepared to describe variations of the major currents. The

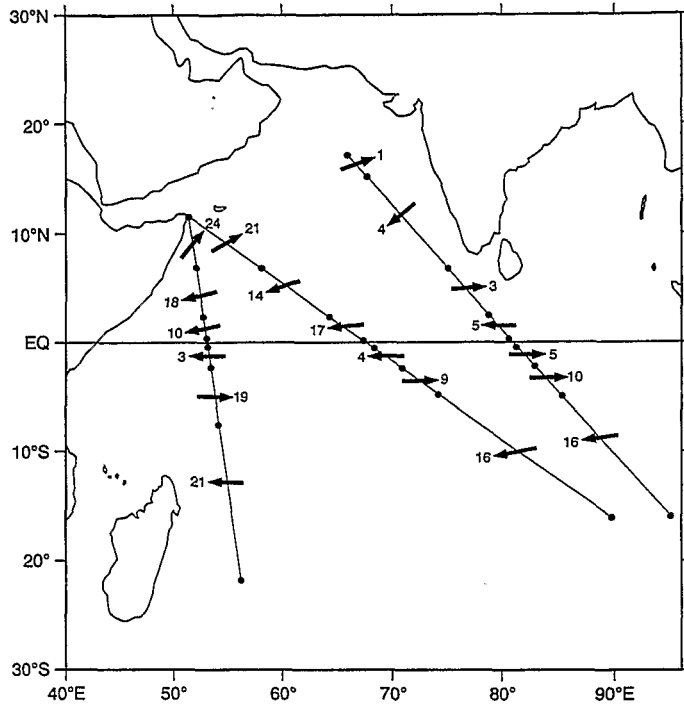


Fig. 7. Transport in Sverdrups ($10^6\text{m}^3/\text{s}$) relative to 400 dB August/September.

annual variations of the Somali Current north of 7.5°N are clearly documented (Fig. 8) on the Red Sea lines. Sampling on the route to the Persian Gulf was unfortunately not permitted close to the coast during the period of this study and the extension of the Somali Current into the northern Arabian Sea could not be monitored. The three lines give a clear representation of variations in the SC and the gyre in the Arabian Sea. The annual cycle of relative transport in the Somali Current on the two Red Sea lines (Fig. 8, left and middle panels) varies from northeastward during May to November with a maximum >20 Sv, to southwestward from November to May with a minimum of 15 Sv. The return flow from the Somali Current circulates around the gyre and crosses the sampled part of the Persian Gulf line flowing in the opposite direction off the southern coast of India (Fig. 8, right panel). The magnitude of variations in the eastern gyre is considerably smaller than in the SC indicating recirculation. The transport variations on the southern side of the gyre on the Reunion–Red Sea line (Fig. 9, left panel) are consistent with the observations of the Somali Current (i.e. the direction is reversed and magnitude about the same). The reversal is also apparent on the Fremantle–Red Sea line (Fig. 9, centre panel), but higher frequency variations also appear.

Annual variation of the NEC/IMC was observed on the Fremantle–Persian Gulf line. The transports (Fig. 9, right panel) were essentially bimodal with westward flow averaging >10 Sv during February through May and eastward flow averaging >5 Sv during July through November. The monsoon variation of surface currents in this region has been noted in earlier studies (Wyrтки, 1973a; Molinari *et al.*, 1990).

The transport of the semiannual eastward jets on the equator (Wyrтки, 1973a; Molinari

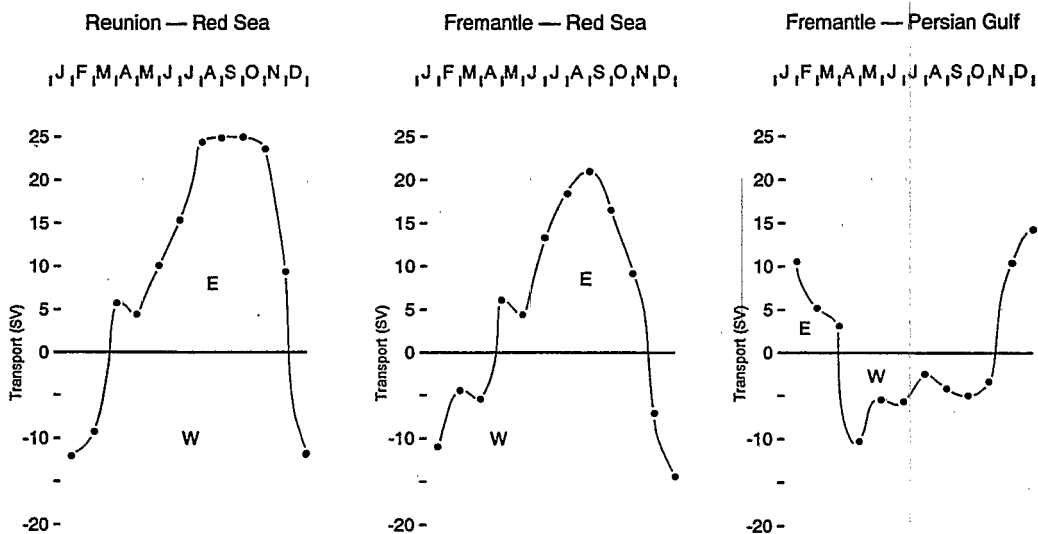


Fig. 8. Transport in Sverdrups ($10^6\text{m}^3/\text{s}$) in the Somali Current, $7.5^\circ\text{--}12.5^\circ\text{N}$, on the Reunion-Red Sea and Fremantle-Red Sea lines; transport between 7.5°N and 15.5°N on the Fremantle-Persian Gulf line.

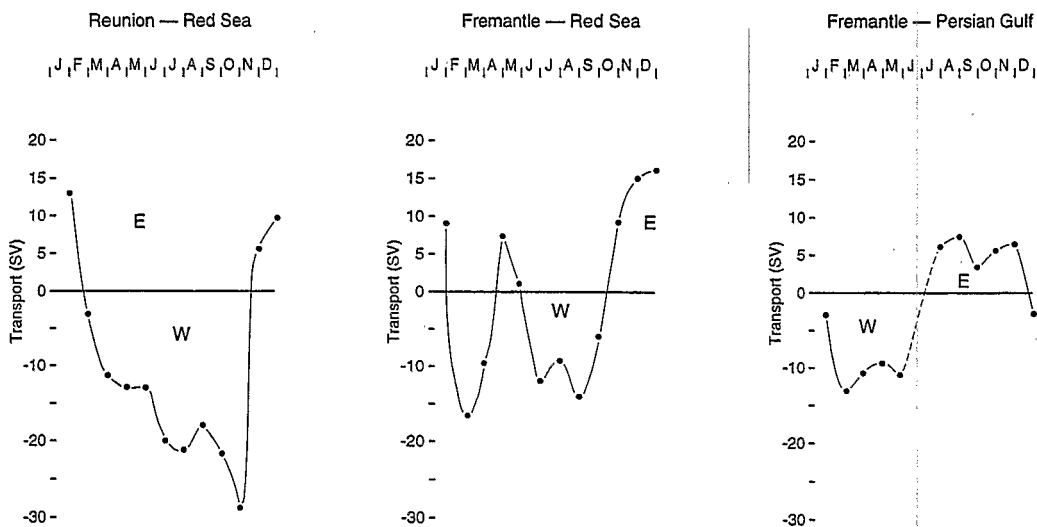


Fig. 9. Transport in Sverdrups ($10^6\text{m}^3/\text{s}$) in the latitude band $2.5^\circ\text{N}\text{--}7.5^\circ\text{N}$.

et al., 1990) were measured separately on either side of the equator. They appear coherently between 2.5°S and the equator (Fig. 10). The time series along the three shipping routes show peaks of eastward transport during the transition seasons with a stronger peak exceeding 15 Sv in the May transition and a weaker peak exceeding 5 Sv in the October transition. Between 2.5°N and the equator (Fig. 11, right panel), the transport

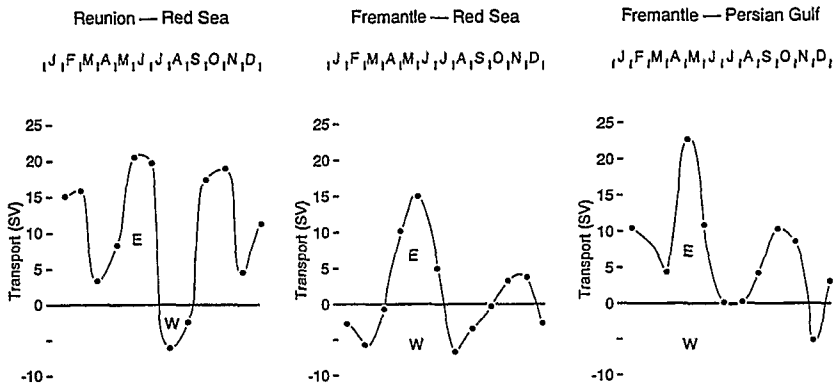


Fig. 10. Transport in Sverdrups ($10^6\text{m}^3/\text{s}$) of the Equatorial Jet in the latitude band 0.5°S – 2.5°S .

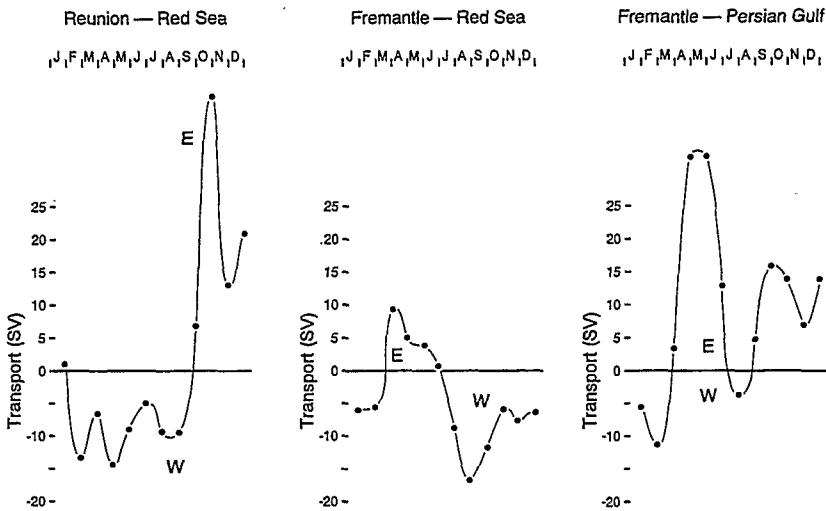


Fig. 11. Transport in Sverdrups ($10^6\text{m}^3/\text{s}$) of the Equatorial Jet in the latitude band 0.5°N – 2.5°N .

on the easternmost line (Fremantle–Persian Gulf) is semiannual and in phase with the jets on the southern side of the equator. The transport on the westernmost line (Fig. 11, left panel) has an annual cycle because it is influenced by the monsoon gyre of the Arabian Sea. Thus it is in phase with the return flow of the Somali Current shown in Fig. 9. Variations on the middle line (Fig. 11, middle panel) have a strong semiannual component in phase with the equatorial jets but the flow becomes dominantly westward during the later part of the year (which we cannot explain or relate to earlier studies).

The SECC is a prominent feature of the southern Indian Ocean circulation and is expected to have an annual cycle associated with the ITCZ. Its transport was calculated between 2.5°S and the Countercurrent trough located between 5° and 10°S , without trying to distinguish it from the equatorial jets. The eastward transport (Fig. 12, top) in the central ocean (Fremantle–Persian Gulf and Fremantle–Red Sea lines) is maximum in April/May when the trough is well developed (Fig. 3). The maximum occurs at the end of

South Equatorial Countercurrent

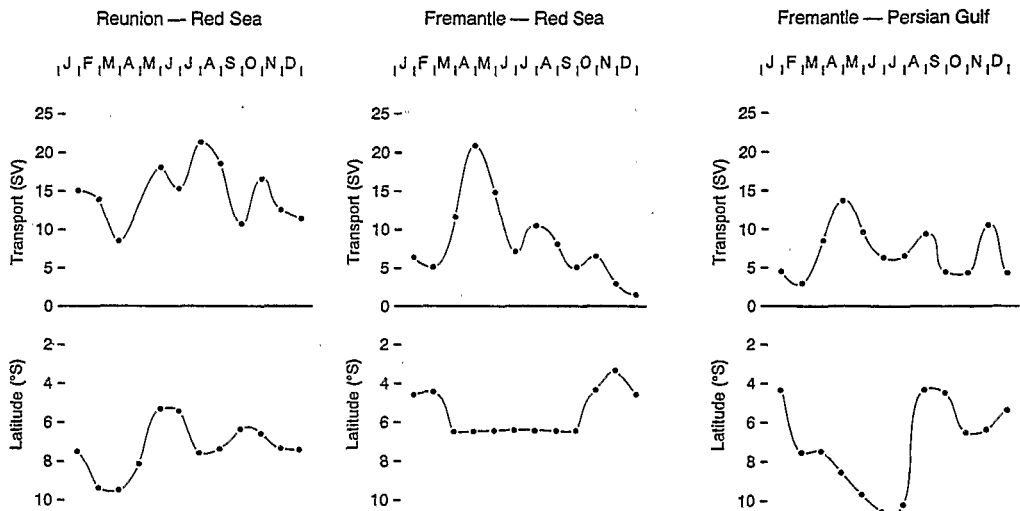


Fig. 12. Transport in Sverdrups ($10^6\text{m}^3/\text{s}$) of the South Equatorial Countercurrent (top) and latitude of the Countercurrent trough (bottom).

Table 2. Mean transport of the South Equatorial Current across the shipping lines of the Indian Ocean

Mean shipping line latitude	Longitude	Transport
Port Hedland–Japan	13°S–9°S	123°E 5.5 Sv
Fremantle–Sunda	15°S–7°S	106°E 9.2 Sv
Fremantle–Persian Gulf	15°S–5°S	93°E 13.4 Sv
Fremantle–Red Sea	17°S–3°S	82°E 18.2 Sv
La Reunion–Red Sea	20°S–7°S	55°E 21 Sv

the season of westerly winds between the equator and 10°S, when the ITCZ is displaced southward. The maximum matches the phase of the May peak of the semiannual equatorial jet (Fig. 10) which probably merges with the SECC at this time. The transport in the western ocean (Reunion–Red Sea line) has a weak maximum somewhat later during June through August and a smaller annual amplitude. The latitude of the trough (Fig. 12, bottom) is between 5°S and 10°S in the westernmost line, between 3°S and 7°S in the central one and varies between 4°S and 11°S in the easternmost line with an abrupt change from 11°S to 4°S between July and August.

The South Equatorial Current is the most powerful and persistent current in the tropical Indian Ocean (Hastenrath and Greischar, 1991) and is easily identified on temperature sections from the topography of the thermocline. Its latitude changes slightly with longitude but remains within the range 5°S–20°S. The transport functions estimated from XBT were used to document the strength of the SEC all across the Indian Ocean (Table 2).

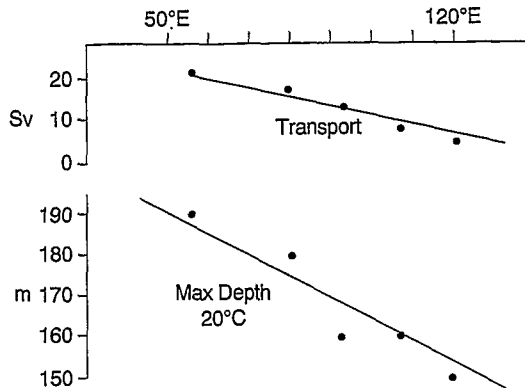


Fig. 13. Increase of the SEC transport from the east to the west and of the 20°C isotherm depths at the southern boundary of the current.

On the Port Hedland–Japan line, the westward flow is between 13°S and 9°S and its mean relative transport is 5.5 Sv at 123°E. On the Fremantle–Sunda Strait line it is between 15°S and 7°S, and has a mean transport of 9.2 Sv at 106°E. (Note that the average covers the eastward South Java Current as well as the SEC in this latitude band. See Meyers *et al.*, 1995 for more details.). On the Fremantle–Persian Gulf line it is between 15°S and 5°S and has a mean transport of 13.4 Sv at about 93°E. On the Fremantle–Red Sea line, it is between 17°S and 3°S, and has a mean transport of 18.2 Sv at about 82°E. On the Reunion–Red Sea line, it is between 20°S and 7°S, and has a mean transport of 21 Sv at 55°E. These values are in good agreement with the SEC transport relative to 400 dB estimated by Hastenrath and Greischar (1991), while reference to a deeper level gives considerably higher values in the range 33–39 Sv (Wyrтки, 1971; Godfrey and Golding, 1981). The deeper observations are larger than the model results of Woodberry *et al.* (1989) due to Indonesian throughflow (Godfrey and Golding, 1981). It is worth noting that the 400 dB transport of the SEC increases from east to west (Fig. 13) as a consequence of the Sverdrup transports generated by wind stress curl. The 400 dB transports are not referenced to a deep enough level to compare quantitatively to the Sverdrup transports (Godfrey, 1989).

The seasonal variation of the SEC transport was estimated along four shipping lines spanning the Indian Ocean (Fig. 14). Only westward flow was counted in the monthly transports, the annual cycle in the eastern Indian Ocean (Fremantle to Sunda Strait route) has a maximum westward transport of 17 Sv in August/September, at the time of maximum westward wind stress in the region. The transport has a distinct semiannual oscillation which Meyers *et al.* (1994a) have associated with the reflection of the equatorial jets along the eastern boundary. A secondary maximum westward transport of 13 Sv is in January/February. In the central Indian Ocean (Fremantle to Persian Gulf route), there is a dominant annual cycle with the maximum in September/October (19 Sv) and the minimum in June/July (12 Sv). Further west (Fremantle to Red Sea route) the transport has a broad maximum from November to January (23 Sv) and a broad minimum between June and August (15 Sv). In the western Indian Ocean (Red Sea to Reunion route), the minimum is in April (18 Sv) and the maximum between October and December (26 Sv). The westward propagation of phase in maximum and minimum transport is associated with the annual Rossby wave in this region described by Perigaud and Delecluse (1993).

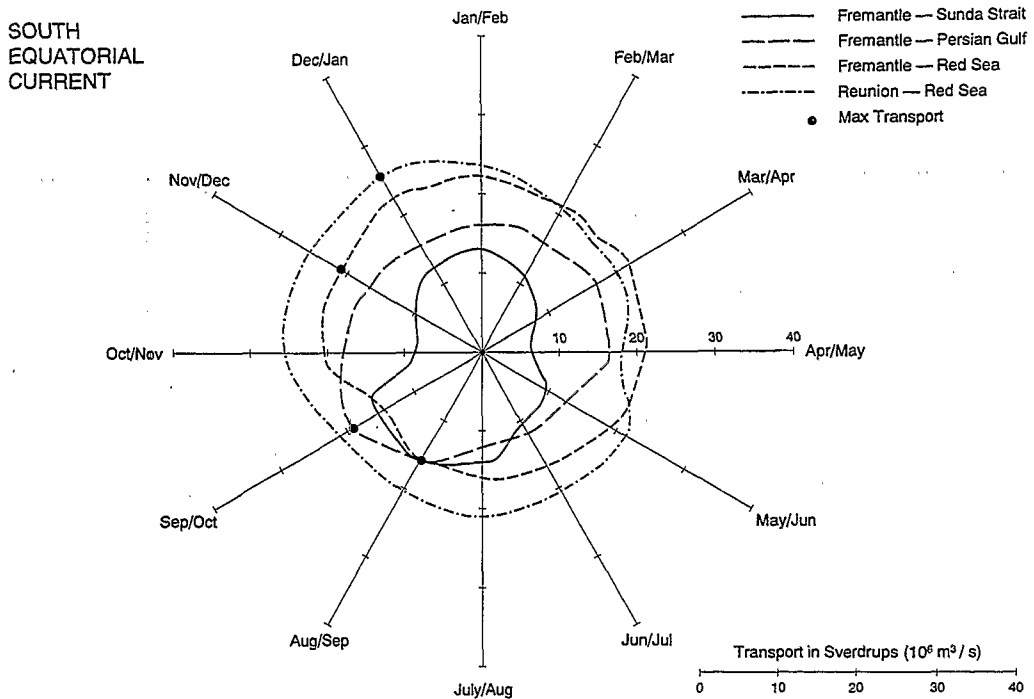


Fig. 14. Annual regime of the South Equatorial Current transport along four routes in the tropical Indian Ocean. The variation of transports in Sverdrups are represented clockwise, with the value for the January/February mean at noon, for April/May at 3 o'clock, etc. The annual maximum transport on each route is indicated by a dot.

Possible inconsistencies in the maps for transport close to the equator (Figs 6 and 7) were noted above. A careful inspection of the temperature sections on the XBT routes suggests that vertical shear and reference level velocities may in part be responsible for inconsistencies in 0–400 m transport. From 5°S to the equator, according to the isotherm pattern for February/March (Fig. 15), there is spreading of the thermocline, similar to the Pacific Ocean, indicating westward transport at the surface and eastward transport below 100 m. On the Red Sea–Reunion and the Red Sea–Fremantle routes during January/February, transport is eastward on either side of the Reunion route and westward on the Fremantle route (Fig. 6). This inconsistency may be due to averaging vertically over the westward and eastward flows at different levels.

6. COMPARISON WITH EARLIER STUDIES

A limited number of recent studies provide a detailed description of the circulation or transports of the major tropical currents in the Tropical Indian Ocean.

Two papers (Reverdin, 1987; Molinari *et al.*, 1990) provide a circulation climatology for the Tropical Indian Ocean from Lagrangian measurements issued from ship drifts or drifting buoys.

Three papers are mostly devoted to the western area of the Tropical Indian Ocean (Swallow *et al.*, 1988; Schott *et al.*, 1988; Swallow *et al.*, 1991). The data used are both

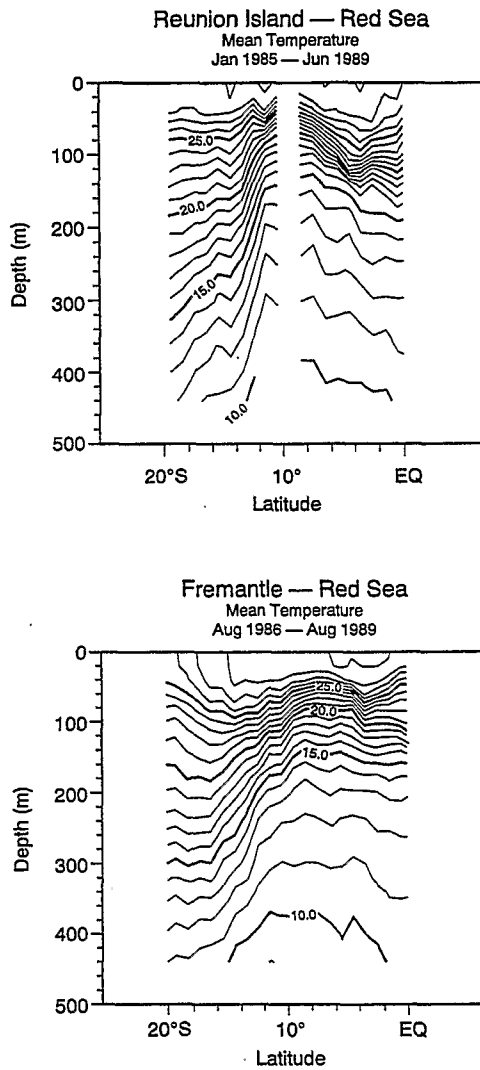


Fig. 15. Vertical temperature section 0–500 m and equator–20°S along the routes Red Sea–Reunion and Red Sea–Fremantle route for February/March.

geostrophic and direct velocity measurements in order to determine the transports of the main currents in the vicinity of Madagascar as well as along the Eastern coast of Africa.

Three papers involve models: one (Woodberry *et al.*, 1989) simulates large scale upper circulation and provides estimation of the transports. Another (Visbeck and Schott, 1992) compares observed data (mooring and ship drift) with results from a model in the western equatorial area. The third one (McCreary *et al.*, 1993) presents, monthly circulation at the surface and in the mixed layer of the entire Tropical Indian Ocean.

One paper (Hastenrath and Greischar, 1991) used XBT and hydrographic casts as basic data, and the resulting transports of some current are directly comparable to the present

study. Transports for SEC and Somali Currents from Woodberry *et al.* (1989) as well as SEC from Swallow *et al.* (1988, 1991) could be also compared. Some fields from McCreary *et al.* (1993) may also be compared to fields from the present study.

1 McCreary *et al.* (1993) (M.C.) versus Donguy and Meyers (D.M.)

The dynamic height field for three typical months from D.M. may be compared to the mixed layer thickness field for the same months from M.C. During April–May, in the southern hemisphere, small dynamic heights coincide with a small mixed layer thickness between the equator and 10°S implying the presence of the SECC and SEC. In the northern hemisphere, the agreement is not so good: large dynamic height (D.M.) is not consistent with small mixed layer thickness (M.C.) at the same location in the Arabian Sea; moreover, the SW monsoon seems to have already started in M.C. but not in D.M.

September from M.C. may be compared to August–September from D.M.: large and small dynamic heights in D.M. seem at the same locations as large and shallow mixed layer in M.C. and the circulation pattern is similar, including eddies in the northern hemisphere.

In January, small dynamic height occurs in both hemispheres and matches well with shallow mixed layer. The circulation patterns in both studies are also in agreement.

According to M.C., the main discrepancy with observations is the failure of the model to reproduce a strong Wyrski Jet in the western basin. For the rest of the basin, the circulations in both studies are mostly in agreement. The discrepancy observed in the northern hemisphere in April–May is probably due to the use in the model (M.C.) of a different wind field than during the observations (D.M.), implying a different starting time of the SW monsoon.

2 Hastenrath and Greischar (1991) (H.G.) versus Donguy and Meyers (D.M.)

Some conspicuous currents studied in the same area may be compared.

In H.G., SEC mean transport is 13 Sv between 60°E and 80°E and from 8°S to 16°S; that is comparable to 18.2 Sv found by D.M. at 82°E relative to the same reference (400 dB) but from 3°S to 17°S and not exactly at the same longitude. In both cases, relatively small seasonal variations are mentioned.

Although the boundaries considered are the same, it is difficult to compare the SECC mean transport because seasonal variations are important: according to H.G., it is about 5 Sv and for D.M., almost 8 Sv in the corresponding area (Fremantle–Red Sea track).

For the Equatorial Eastward Jet, important in May and November, H.G. find 14 Sv in May for both sides of the equator combined, D.M. find 10 Sv north of the equator and 15 Sv south of the equator, that is, much stronger. In November, in the considered area, H.G. give 12 Sv and D.M. 5 Sv, but only in the southern hemisphere.

The South West Monsoon Current (S.W.M.) from H.G. coincides with the Indian Monsoon Current (I.M.C.) from D.M. Mean westward transport of S.W.M. is 3 Sv, whereas mean westward transport of I.M.C. is 5 Sv.

Transports from H.G. and D.M. are in fact very different, because the data sets are not similar: most of the observations from H.G. are hydrographic casts collected mostly during 1963–1984, whereas data from D.M. are only XBT collected after this period. The methods of the transport calculation are also different: D.M. use only geostrophic flow; H.G. include Ekman and geostrophic flows. For SEC and SECC, Ekman transport is

negligible compared to the geostrophic one, but it is relatively important for EEJ and SMC. Moreover, for EEJ, the equatorial calculation of the geostrophic transport close to the equator could be questionable.

3 Woodberry et al. (1989) versus Donguy and Meyers

According to the Woodberry model, northeastward transport of the Somali Current is 18 Sv, and southwestward transport is 7 Sv but with only 200 metres reference depth, whereas D.M. find respectively 20 Sv and 15 Sv with 400 metres reference depth.

SEC at 63°E has a transport of 24 Sv from 8°S to 23°S and a transport of 17 Sv at 49°E from 10 to 12°S for Woodberry with 200 metres reference, whereas SEC transport for D.M. is 21 Sv at 55°E from 7°S to 20°S. Considering the difference of reference level, the transport from D.M. is considerably smaller than the one derived from the model.

4 Swallow et al (1988, 1991) versus Donguy and Meyers

Swallow *et al.* from current measurements as well as dynamic heights, both relative to 700 metres depth, find 25 Sv for SEC transport at 50°E north of Madagascar, that is comparable to 21 Sv at 55°E relative to 400 metres from M.D.

Table 3 gives a summary of the transports presented by each study, particularly for the Somali Current, Indian Monsoon Current (IMC), Equatorial Eastward Jet, South Equatorial Countercurrent (SECC) and the South Equatorial Current (SEC).

There are many discrepancies between D.M. and the previous studies, the most coherent values being the SEC transport. That is not surprising because periods, areas, current boundaries and methods are all different. The most similar is H.G. which used the same kind of data but gathered during a different period. However the present study (D.M.) is the only one to present the transport regime of the major currents over a great part of the Indian Ocean with calculations from an homogeneous data set.

7. CONCLUSION

Studies of the large scale oceanographic conditions in the Indian Ocean have been rare until the present time, due to lack of data. the French–Australian TOGA XBT network provides an opportunity to document the thermal, baroclinic variability. Seasonal variations have been first investigated in a preliminary climatology based on data collected during the first half of the TOGA Programme. While a climatology based on many more observations will be possible at the end of TOGA, this first attempt has provided representative and quantitative measures of the transport of major currents, which previously were described qualitatively from surface drift data. The study confirms that in the western Indian Ocean currents and transports have a strong annual variation related to the monsoon regime. Interannual variations will be the subject of a further study.

Acknowledgements—Volunteer observers on merchant ships have generously collected the data in the field. Substantial external resources were provided by Royal Australian Navy, Department of the Environment (Australia), Bureau of Meteorology (Australia), NOAA (USA), Department of Education (Japan) and Japan Meteorological Agency. R.J. Bailey is the scientist-in-charge of the CSIRO Ocean Observing Networks. M.

Table 3. Comparison of the present study with earlier ones

	Period	Area	Method	Data	7°.5N-12°.5N Somali Current	2°.5N-7°.5N IMC SWM	0.5S-2.5S Eastward Jet	0.5N-2.5N Eastward Jet	SECC	SEC
McCreary <i>et al.</i> , 1993		29°S-25°N	Model	Wind heat fluxes air temperat.						
		35°E-115°E								
Visbeck and Schott, 1992	1979-80	0° 47°E-59°E	Mooring model	Current						
Woodberry <i>et al.</i> , 1989		25°S-26°N 35°E-125°E	Model H ₀ = 200 m	Wind	4°-5°N 49°E NE 18 Sv SW 7 Sv					63°E 24 Sv 49°E (10°S-12°S) 17 Sv
Swallow <i>et al.</i> , 1988-1991	1963-75 1984-86	24°S-4°S 40°E-52°E	Mooring Geostrophic Currents	Current ADCP CTD XBT						50°E Current 24.8 Sv/700 Geostroph 25.5 Sv/700
Hastenrath and Greischar, 1991	1963-84	25°S-25°N 35°E-90°E	Geostrophic Current relative to 400 db	CTD XBT		W 3 Sv (mean)	May 14 Sv		60°-80°E 5 Sv (mean)	60°-80°E 13 Sv (mean)
Donguy and Meyers	1985-89	25°S-15°N 50°E-100°E	Geostrophic Current relative to 400 db	XBT	NE 20 Sv SW 15 Sv	E > 5 Sv W > 10 Sv	May > 15 Sv Oct > 5 Sv	May 10 Sv	May 20 Sv Mean 8 Sv	82°E 18.2 Sv (mean) 55°E 21 Sv (mean)

Prive is in charge of ORSTOM observations in Le Havre. A. P. Worby was the programmer for development of the climatology and L. Pigot calculated the EOFs. We gratefully acknowledge all of this support.

REFERENCES

- Colborn J. G. (1975) *The thermal structure of the Indian Ocean*. University of Hawaii Press, Honolulu, 173 pp.
- Donguy J. R. (1974) Une année d'observations de surface dans la zone de mousson de la partie occidentale de l'Océan Indien. *Cahiers ORSTOM Serie Oceanographie*, **12**, 2, 118–128.
- Donguy J. R. and B. Piton (1991) The Mozambique Channel revisited. *Oceanologica Acta*, **15**, 549–558.
- Donguy J. R. and G. Meyers (1992) Zonal surfaces current distribution in the tropical Indian Ocean from XBT TOGA network. *TOGA Notes*, **July 1992**, 7–11.
- Duing W., R. L. Molinari and J. C. Swallow (1980) Somali Current: evolution of surface flow. *Science*, **209**, 588–590.
- Godfrey J. S. (1989) A Sverdrup model of the depth integrated flow for the world ocean allowing for island circulations. *Geophysic and Astrophysic Fluid Dynamics*, **45**, 89–112.
- Godfrey J. S. and T. J. Golding (1981) The Sverdrup relation in the Indian Ocean and the effect of Pacific–Indian circulation and on the East Australian Current. *Journal of Physical Oceanography*, **11**, 771–779.
- Hastenrath S. and L. Greischar (1991) The monsoonal current regimes of the Tropical Indian Ocean. Observed surface flow fields and their geostrophic and wind-driven components. *Journal of Geophysical Research*, **96**, 12619–12633.
- Knox R. A. (1987) The Indian Ocean: Interaction with the Monsoon. In: *Monsoons*, J. S. Fein and P. L. Stephens, editors, Wiley, New York, pp. 365–397.
- Ku H. H. (1966) Notes on the use of propagation of error formulas. *Journal of Results of the National Bureau of Standards—C. Engineering and Instrumentation*, **70C**, 331–341.
- Levitus S. (1982) *Climatological Atlas of the World Ocean*. NOAA, Professional Paper No. 13, US Department of Commerce, 173 pp.
- McCreary J. P., P. K. Kundu and R. Molinari (1983) A numerical investigation of dynamics, thermodynamics and mixed-layer processes in the Indian Ocean. *Progress in Oceanography*, **31**, 181–244.
- Meyers G. (1979) On the annual Rossby wave in the tropical North Pacific Ocean. *Journal of Physical Oceanography*, **9**, 663–674.
- Meyers G. (1992) Indian Ocean Analyses. In: *Proceedings of the Ocean Climate Data Workshop*, Goddard Space Flight Center, Greenbelt, pp. 109–129.
- Meyers G., H. Phillips, N. Smith and J. Sprintall (1991) Space and time scales for optimal interpolation of temperature in the tropical Pacific Ocean. *Progress in Oceanography*, **28**, 189–218.
- Meyers G. and H. Phillips (1992) TOGA XBT sampling strategy. *TOGA Notes*, **April 1992**, 16–21.
- Meyers G., R.J. Bailey and A.P. Worby (1995) Geostrophic transport of the Indonesian throughflow. *Deep-Sea Research* (submitted).
- Meyers G., R. J. Bailey and A. P. Worby (1994b) *Working atlas of thermal structure on TOGA XBT lines in the Indian Ocean*. CSIRO Marine Laboratories Internal Report (Unpublished manuscript).
- Molinari R. L., D. Olson and G. Reverdin (1990) Surface current distributions in the Tropical Indian Ocean derived from compilations of surface buoy trajectories. *Journal of Geophysical Research*, **95**, 7217–7238.
- Perigaud C. and P. Delecluse (1993) Annual sea level variations in the southeastern tropical Indian Ocean. *Journal of Geophysical Research*, **97**, 20169–20178.
- Phillips H., R. Bailey and G. Meyers (1990) *Design of an ocean temperature observing network in the seas north of Australia, Part II tropical Indian Ocean: statistics*. CSIRO Marine Laboratories Report No. 211, 58 pp.
- Reverdin G. (1987) The upper equatorial Indian Ocean: the climatological seasonal cycle. *Journal of Physical Oceanography*, **17**, 903–927.
- Sadler J. C., M. A. Lander, A. M. Huri and L. A. Oda (1987). *Tropical marine climatic atlas, Vol 1, Indian and Atlantic Ocean*, NOAA, Department of Meteorology, University of Hawaii.
- Schott F., M. Fieux, J. Kindle, J. Swallow and R. Zantopp (1988) The boundary currents east and north of Madagascar, 2. Direct measurements and model comparisons. *Journal of Geophysical Research*, **93**, 4963–4974.
- Swallow J. C. and M. Fieux (1982) Historical evidence for two gyres in the Somali Current. *Journal of Marine Research*, **40**, Suppl 747–755.
- Swallow J. C., M. Fieux and F. Schott (1988) The boundary currents east and north of Madagascar, 1. Geostrophic currents and transports. *Journal of Geophysical Research*, **93**, 4951–4962.

- Swallow J. C., F. Schott and M. Fieux (1991) Structure and transport of the East African Coastal Current. *Journal of Geophysical Research*, **96**, 22245–22257.
- Taft B. A. and W. S. Kessler (1991) Variations of zonal currents in the central tropical Pacific during 1970 to 1987: Sea level and dynamic height measurements. *Journal of Geophysical Research*, **96**, 12599–12618.
- Visbeck M. and F. Schott (1992) Analysis of seasonal Current variations in the Western Equatorial Indian Ocean. Direct measurements and GFDL model Comparison. *Journal of Physical Oceanography*, **22**, 1112–1128.
- Woodberry K. E., M. E. Luther and J. O'Brien (1989) The wind-driven seasonal circulation in the Southern Tropical Indian Ocean. *Journal of Geophysical Research*, **94**, 17985–18002.
- Wyrtki K. (1971) *Oceanographic atlas of the international Indian Ocean expedition*, National Science Foundation, Washington DC, 531 pp.
- Wyrtki K. (1973a) *Physical Oceanography of the Indian Ocean*. In: *Ecological Studies—Analysis and Synthesis*, Vol. 3, B. Zeitzchel, editor, Springer-Verlag, Berlin, pp. 18–36.
- Wyrtki K. (1973b) An equatorial jet in the Indian Ocean. *Science*, **181**, 262–264.